Journal of Sound and Vibration (1999) **223**(1), 115–140
Article No. jsvi.1998.2099, available online at http://www.idealibrary.com on IDEAL®

STOCHASTIC DYNAMICS OF SYSTEMS WITH FRICTION-INDUCED VIBRATION

S. L. Qiao and R. A. Ibrahim
Department of Mechanical Engineering, Detroit, MI 48202, *U.S.A.*

(*Received* 16 *October* 1998, *and in final form* 16 *December* 1998)

This paper presents linear and non-linear phenomenological models of interfacial forces between a rotating disc and a rigid pin in contact with the disc. The models are developed based on experimental results which revealed that both normal and frictional forces were essentially random non-Gaussian processes. The characteristics of these forces are different when the disc reverses its rotation. When the disc rotates clockwise, the sprag-slip phenomenon occurs due to so-called kinematic constraint instability. Furthermore, in view of the time variations of contact forces, the boundary conditions of the pin become time varying and its natural frequency becomes time-dependent. The interfacial forces appear in the pin's equation of motion as multiplicative and non-homogeneous terms. In the non-linear model, the normal force appears as multiplicative of velocity terms up to cubic order. The pin's dynamic behavior was studied using the method of stochastic averaging. For the non-linear model, the problem of noise-induced transition was examined for clockwise and counter-clockwise cases. The pin amplitude extrema were found to be more complex for the case of clockwise rotation than those for the counter-clockwise case. For the linear model, the complete probabilistic description of the pin's dynamic behavior is derived in a closed form in terms of disc speed and friction power spectral density level.

1. INTRODUCTION

Friction-induced noise is usually encountered in power control components such as vehicle braking systems, friction clutches, and friction belts. Other occurrences include machine tool vibration, stern-tube water-lubricated bearing vibration in submarines, and wheel/rail squeal in mass transit systems. When the kinetic friction coefficient depends strongly on the sliding velocity and possesses a negative slope with respect to the velocity, the friction gives rise to *negative damping*. In this case the friction may develop different types of instability such as stick-slip, quasi-harmonic oscillation (or limit cycle) [1–3], chaos [4, 5], chatter, and squeal [6, 7]. Stick-slip oscillation is characterized by a saw-tooth displacement curve. Stick-slip motion is governed by static and kinetic friction forces. The quasi-harmonic motion has a near-sinusoidal displacement–time curve and the motion is initiated and maintained by kinetic friction force.

0022–460X/99/210115 + 26 $30.00/0

Friction phenomena of an audible nature, including chatter and squeal, can occur in systems with sliding parts, and each occurs within a certain frequency band. (For example, high-frequency noise is termed squeal, and low-frequency noise is called chatter.) This is mainly due to the inherent non-linearities of contact forces, which are important factors in generating these types of noises. It appears that audible noises are generated intermittently and without any apparent order or combination. However, when their frequencies are analyzed and studied in detail, one may find that such noises are generated in combination. In some cases parametric resonances can take place, as reported by Mottershead *et al*. [8].

Contact forces between sliding surfaces arise due to complex mechanisms, and lead to mathematical models which are strongly non-linear, discontinuous, and non-smooth. The inclusion of such non-linearities in the equations of motion of a dynamical system can have interesting effects on the dynamic response characteristics. This non-linearity leads to *differential inclusions* in the mathematical model [9], adding further difficulty to the problem. Differential inclusions can be regarded as differential equations that consist of set-valued or multi-valued terms. Accordingly, the existence and uniqueness of solutions are no longer guaranteed, except in a few cases [10].

Experimental tests on a pin-on-disc type sliding system [11] have indicated that the friction force depends on the normal load for a constant sliding speed. Depending on the value of the normal load, four different friction regimes have been observed. These are (1) the steady-state friction region where the frictional force increases linearly with the normal load; (2) the non-linear friction region in which the friction force increases non-linearly with the normal load and the coefficient of friction is no longer constant but increases with the normal load; (3) the transient region characterized by intermittent variation of the friction force. When the mean friction force reaches a sufficiently high value, a temporary burst of self-excited vibrations occurs and the friction force falls to a low value; (4) the self-excited vibration region where the mean friction force drops to a very low value and is accompanied by high amplitude periodic self-excited oscillations. The first two regimes are characterized by small amplitude random vibrations of the slider in the tangential, normal, and torsional degrees of freedom. In the self-excited vibration regime, the normal load results in an unstable limit cycle. The source of such limit cycles is the non-linearity due to non-linear contact forces, and to coupling between the degrees of freedom.

These experimental results did not address the effect of the sprag-slip phenomenon. This phenomenon was defined by Spurr [12] to explain the contact behavior of internal and external drum and disc brakes. It takes the form of locking a body in contact with a sliding surface, followed by a slip due to a displacement of the fixed end of the body. This is known as geometrically-induced or kinematic constraint instability, which occurs even though the coefficient of friction is constant. Sprag-slip results in squeals which occur at numerous frequencies, implying non-linearity. Sudden jumps in frequency during a single squeal are accompanied by simultaneous changes in the friction coefficient. Very often, squeal depends on the magnitude of the friction

coefficient, not on the friction force, and is associated with rapid oscillations in the friction coefficient. This phenomenon motivated the authors to conduct a series of experiments on a pin–disc model to characterize the interfacial forces between the pin and the rotating disc. The measured normal and friction forces were essentially random processes, but with different features when the disc reverses rotation [13]. The dependence of the root mean square of the friction force on the relative velocity for clockwise rotation was different from that obtained for counter-clockwise rotation.

Based on the experimental results of Ibrahim *et al.* [13], an analytical stochastic model is presented emulating the experimental model. This paper presents a stochastic analysis of two different friction models. In the non-linear model, the friction force appears as a multiplicative term to non-linear velocity terms up to cubic-order. The method of stochastic averaging is used to examine the problem of noise-induced transition. The other model is essentially piecewise linear, and the method of stochastic averaging yields a complete description of the probabilistic behavior of the friction element.

2. BRIEF REVIEW OF EXPERIMENTAL RESULTS

A series of experimental tests was conducted on a disc–pin apparatus system shown schematically in Figure 1, together with signal transducers and other equipment. One important requirement of friction-induced vibration is to conduct tests at relatively low speeds. However, when operating at a relatively low rpm, it was observed that the rotor speed experienced substantial fluctuations even under no loading. This type of motor achieves steady speeds only at a relatively high speed. Accordingly, a 10:1 rpm ratio between the motor and the rotor was introduced through a velocity reduction pulley set. The application of velocity reduction yields large torque output by the motor at high speed, and minimizes speed fluctuations. There was also some inevitable misalignment, which resulted in a 0·05-mm level difference of the ring surface at a radius of 0·065 m.

The vibration of the friction element assembly was measured using a one-dimensional accelerometer. The measured acceleration was integrated once to give the velocity of the friction element. The relative velocity of the friction element with respect to the disc speed was estimated as $V_{rel} = V_R - V_f$, where V_R is the average angular velocity times disc radius, and V_f is the velocity of the friction element. The normal and tangential components of the contact force between the friction element and the disc were measured using a three-dimensional Kistler 9251 force transducer. The signals from the transducers were processed through a D/A converter Data Translation EZ 8-channel D/A board. The sampling rate was 500 Hz over 60 s time duration for each test. DT VEE 3.0 software was used for data processing and statistical parameter estimates.

The ideal design of two sliding surfaces requires perfect mating of the surfaces and orthogonality with the rotational axis. However, there is inevitable misalignment resulting from imperfect machining and assembly of the system components. There are three sources of misalignment and surface irregularities:

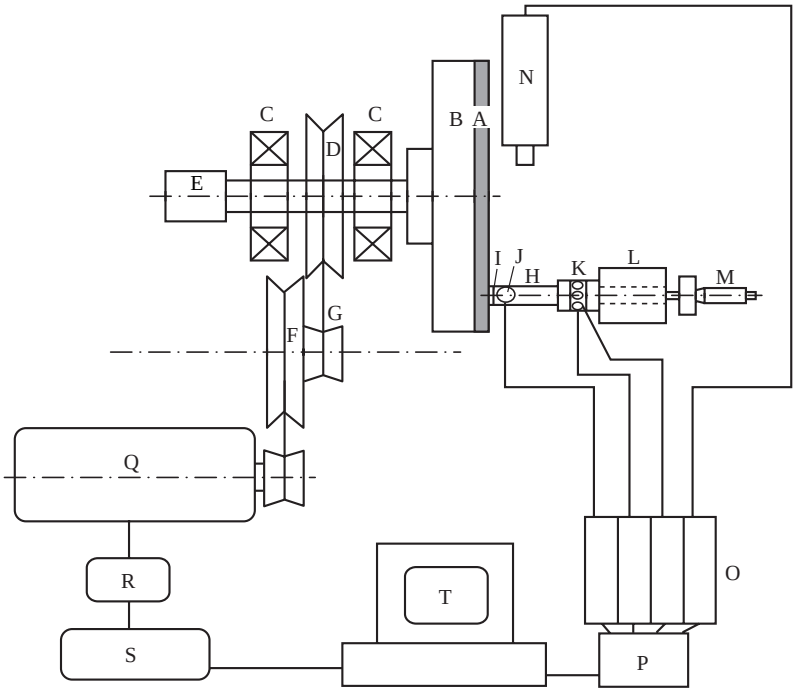

Figure 1. Schematic diagram of the experimental model and equipment: A: friction disc, B: rotor, C: bearings, D: V groove pulley, E: optical encoder, F: speed reduction pulley set, G: V belt, H: friction element, I: 1/4″ dowel pin, J: accelerometer, K: 3-dimensional force transducer, L: slider set, M: micrometer, N: laser transducer, O: signal amplifier, P: A/D converter, Q: compumotor, R: noise filter, S: motor controller, T: PC computer.

(1) the friction element's horizontal axis is not perfectly horizontal and may have a non-zero angle. (2) The disc surface is not exactly orthogonal to the rotational axis, which results in an angle different from 90°. The resultant of the two angles will create an angle of attack θ. (3) The disc surface is not perfectly flat, but contains irregularities in the form of hills and valleys due to the regenerative effect of machining. This effect may result in loss of contact in some spots and contact in other regions, resulting in periodic variations of the normal force and time variations superimposed on θ. When the disc rotates clockwise, the angle of attack between the friction element and the disc surface is usually less than 90°. On the other hand, if the rotation is counter-clockwise the angle of attack becomes greater than 90°. It is clear that if θ is less than 90° the mechanism of sprag-slip is created due to the generation of a strong restraining force between the disc and the friction element. The friction element may experience severe friction-induced vibrations at an attack angle less than 90°. The surface asperities only lead to an additive small random component to the normal load.

The measured results include time history records of normal and friction forces, the acceleration of the friction element, and the coefficient of friction of a friction element sliding on a rotating disc. These results were obtained for clockwise and counter-clockwise disc rotations and are completely reported in reference [13]. This section presents one sample of the results for clockwise and counter-clockwise disc rotations.

Figure 2(a) shows time history records of normal and friction forces, the coefficient of friction, and the acceleration of the friction element for disc speed 3 rpm clockwise. Due to misalignment, the kinematic constraint takes place with clockwise rotation. The normal force was initially set at 55 N. However, the normal force time history records reveal irregular fluctuations, with occasional non-contact zones when the friction element loses contact with the disc surface. As the constraint force increases due to hills on the disc surface, the normal force increases and the friction force increases as well. The plotted friction coefficient is estimated as the ratio of friction force to the normal force. One might expect this ratio to be constant over the duration of the test. However, the friction coefficient records display random fluctuations, and do not remain constant. These fluctuations may be attributed to the fact that the relative velocity is always fluctuating, and thus results in a corresponding variation in the friction coefficient. There is a switch in the friction force, associated with a corresponding change in the relative velocity direction. The power spectral density function of the friction element acceleration is shown in Figure 2(b). There is no unique peak in the spectra, indicating that the natural frequency of the friction element is always changing with time. The time variation of the natural frequency is attributed to the time variation of the boundary conditions (contact forces). Figure 2(c) shows the probability density function (pdf) of the friction force which is essentially non-Gaussian. The Gaussian distribution is plotted in order to realize how the measured friction distribution is deviated from normality.

When the disc rotation is reversed to counter-clockwise, the angle of attack becomes greater than 90°. Accordingly, the constraint force is not significant and the interfacial forces experience high frequency fluctuations over those disc zones with surface hills. In the absence of hills, the friction force is almost constant. Figure 3(a) shows the time history records at 3 rpm of contact forces, friction coefficient and friction element acceleration. The contact forces exhibit slight random fluctuations over almost half of the disc. The friction force is always positive indicating that the relative speed does not change direction. Figure 3(b) shows the power spectral density function of the friction element acceleration. The spectrum of the friction element acceleration exhibits peaks at around 50 and 100 Hz, with surrounding spikes. This means that the contact forces have significant effects on changing the frequency content of the friction element. Figure 3(c) shows the probability density function of the friction force, with long tails to the right indicating asymmetry in the pdf.

Since the friction coefficient and the relative velocity vary randomly with time, the root mean square (rms) of each was estimated for six tests running at 1- through 6 rpm. The friction coefficient–velocity curves for clockwise and counter-clockwise disc rotations are shown in Figure 4. The friction–velocity curve for the clockwise case has a higher negative slope at low values of relative speed than the counter-clockwise case. The stochastic analytical modelling based on these experimental measurements is developed in the next section.

3. ANALYTICAL MODELLING

The analytical modelling consists of a rigid bar with its free end facing the disc while the other end is attached to a torsional spring of stiffness k_θ, replacing the load cell, as shown schematically in Figure 5. The end of the bar in contact with the disc is subjected to contact normal, $N(t)$, and tangential, $F(t)$, random forces. For a small angle θ, the governing equation of motion of the bar can be obtained by summing moments about O as

$$\ddot{\theta} + 2\zeta\omega_0\dot{\theta} + [\omega_0^2 - \alpha(t)]\theta = -\beta(t), \tag{1}$$

where $\omega_0 = \sqrt{k_\theta/I_0}$, $\alpha(t) = LN(t)/I_0$, $\beta(t) = LF(t)/I_0$, m is the mass of the bar, L is the length of the bar, g is the acceleration due to gravity, i_0 is the mass moment of inertia of the bar about the point O, and θ is the rotational angle of the bar measured from the static equilibrium position θ_0. A linear viscous

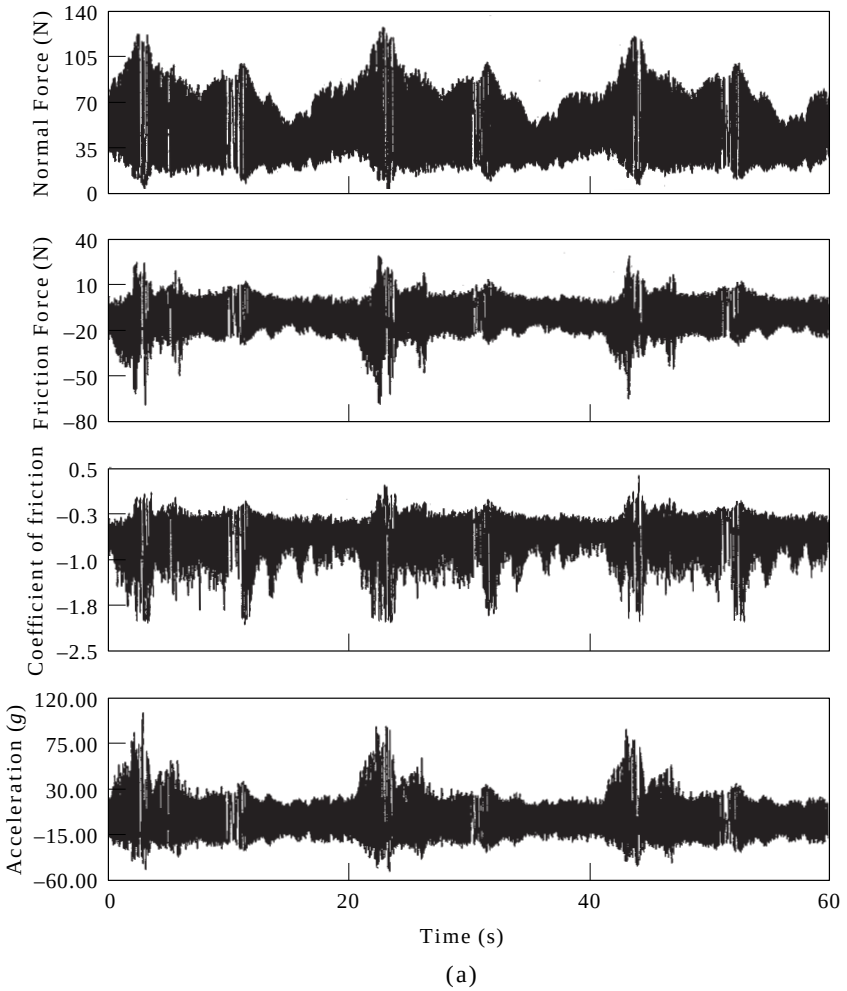

(a)

Figure 2(a) (*caption opposite*)

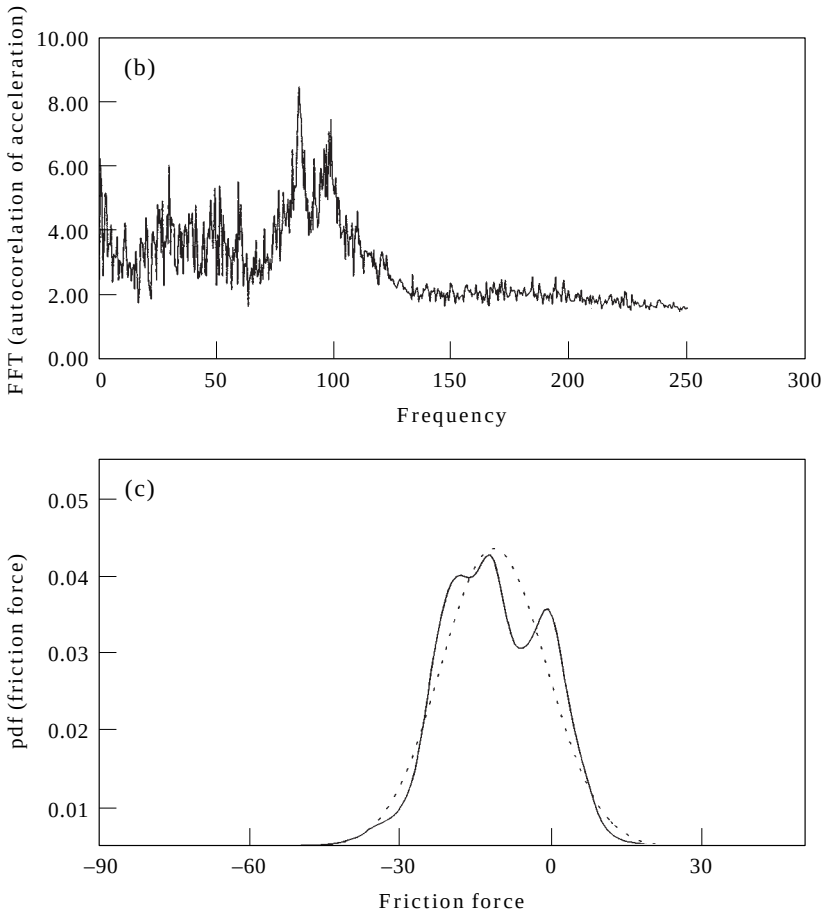

Figure 2. Contact forces characteristics for disc speed of 3 rpm clockwise. (a) Time history records of normal and friction forces, coefficient of friction, and friction element acceleration. (b) Power spectral density of friction element acceleration. (c) Probability density function of the friction force (————, measured curve; – – –, Gaussian curve).

damping term has been introduced to account for energy dissipation. The tangential force $F(t)$ is not independent of the normal force. Furthermore, based on the experimental results, one may approximate the contact forces by random processes with wide band spectral density function. This approximation will overcome the difficulties encountered with the problem of *differential inclusions* in the mathematical modelling. The dependence of the friction coefficient on the relative sliding velocity, shown in Figure 4, may be represented by the cubic polynomial

$$\mu = a_0 \operatorname{sgn}(V - \dot{y}) - a_(V - \dot{y}) + a_3 (V - \dot{y})^3, \tag{2}$$

where V is the disc tangential velocity at the contact point and $\dot{y} = L\dot{\theta}$ is the velocity of the frictional element at the same point of contact. The coefficients

a_0, a_1 and a_3 are determined from the experimental measurements shown in Figure 4. These coefficients are mainly governed by the conditions of the sliding surfaces and their material properties. By applying the least-square curve fitting to the data measured, one obtains the particular form of relation (2) as follows: (1) For counter-clockwise disc rotation (CCW) $a_0 = 0{\cdot}52694$, $a_1 = 14{\cdot}1718$, $a_3 = 5569{\cdot}68$, and

$$\mu = 0{\cdot}52694\ \mathrm{sgn}(V - \dot{y}) - 14{\cdot}1718(V - \dot{y}) + 5569{\cdot}68(V - \dot{y})^3. \tag{3a}$$

(2) For clockwise disc rotation (CW) $a_0 = 1{\cdot}88741$, $a_1 = 79{\cdot}087$, $a_3 = 26212{\cdot}4$ and

$$\mu = 1{\cdot}88741\ \mathrm{sgn}(V - \dot{y}) - 79{\cdot}087(V - \dot{y}) + 26212{\cdot}4(V - \dot{y})^3. \tag{3b}$$

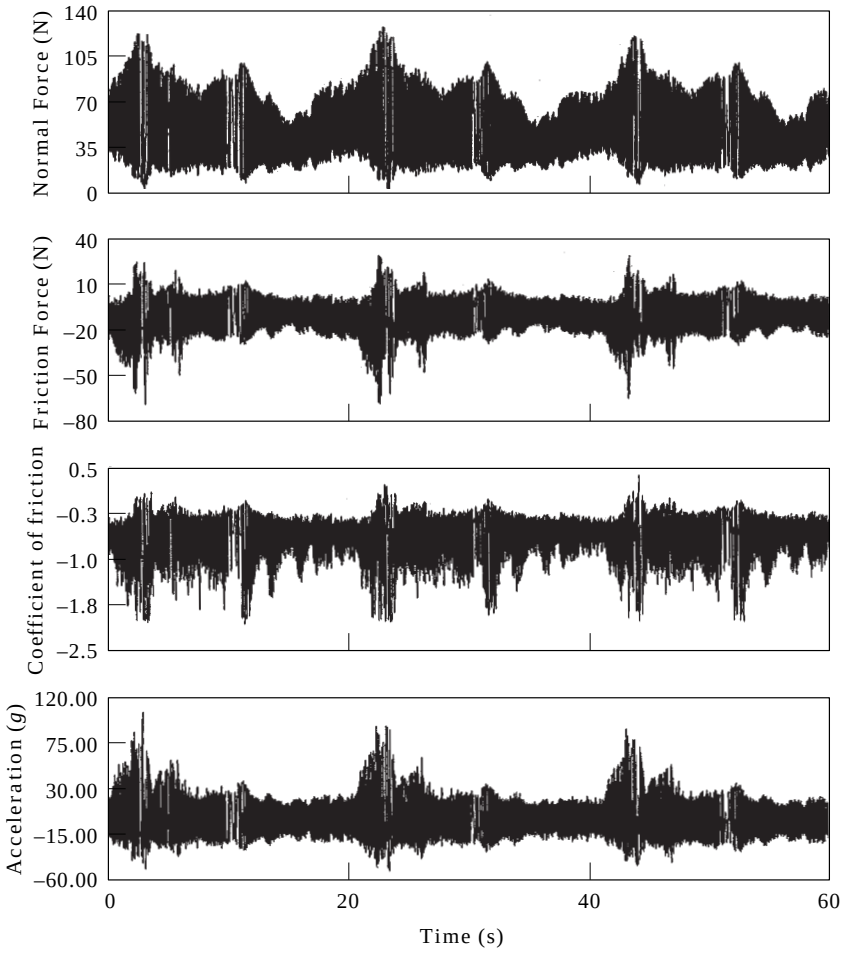

(a)

Figure 3(a) (*caption opposite*)

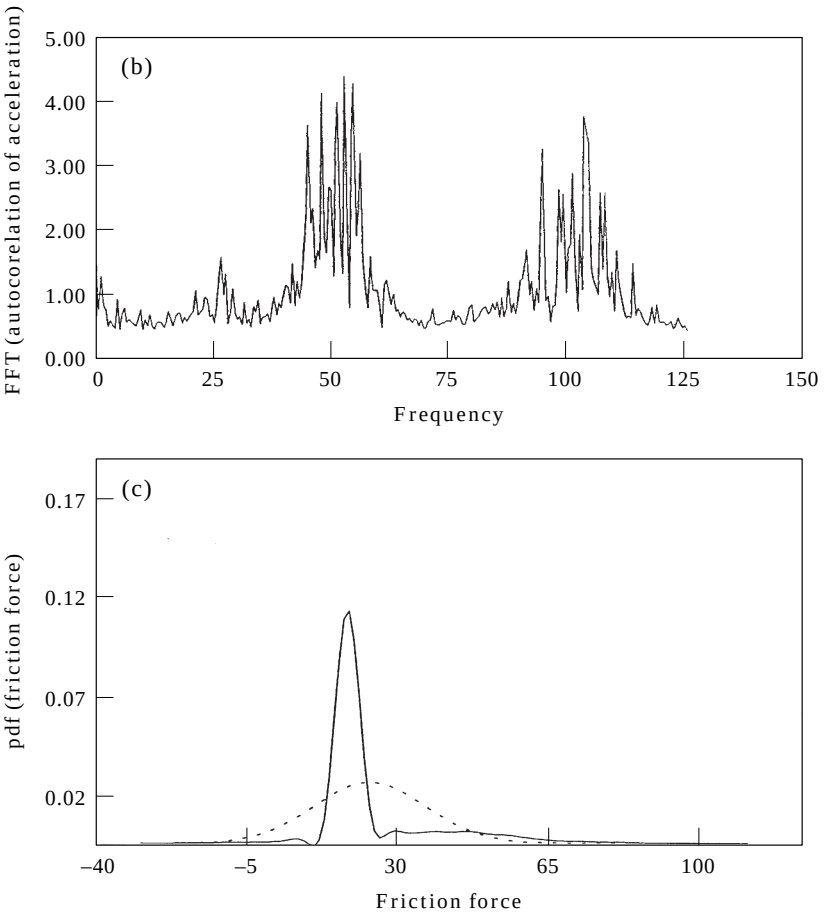

Figure 3. Contact forces characteristics for disc speed of 3 rpm counter-clockwise. (a) Time history records of normal and friction forces, coefficient of friction, and friction element acceleration. (b) Power spectral density of friction element acceleration. (c) Probability density function of the friction force (————, measured curve; – – –, Gaussian curve).

This is shown in Figure 6. In this case, the relationship between friction, $\beta(t)$, and normal, $\alpha(t)$, forces can be written in the form

$$\beta(t) = [a_0 \operatorname{sgn}(V - \dot{y}) - a_1(V - \dot{y}) + a_3(V - \dot{y})^3]\alpha(t). \tag{4}$$

Note that a_0 can be regarded as a static friction coefficient, in that μ will reach its maximum when $(V - \dot{y}) = 0$. Furthermore, the friction–velocity curve possesses negative slopes when $(V - \dot{y}) < \sqrt{a_1/3a_3}$, and positive slopes when $(V - \dot{y}) > \sqrt{a_1/3a_3}$. This feature will have an important effect on the dynamic behavior of the system. Under the condition $V \gg \dot{y}$ one can set $\operatorname{sgn}(V - \dot{y}) = +1$.

A simplified model, referred to as piecewise linear, can be obtained by removing the cubic term of the relative velocity from equation (2). This model is obtained by curve-fitting with the result shown in Figure 7. The corresponding analytical expressions are

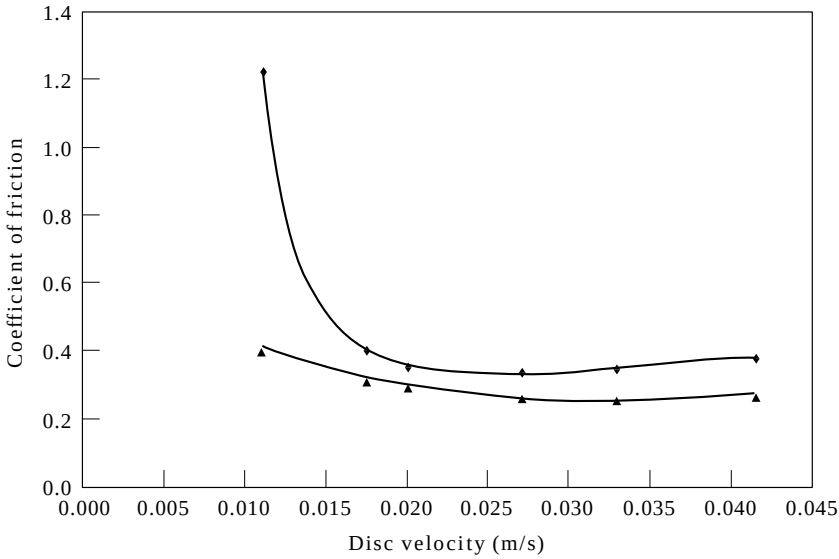

Figure 4. Coefficient of friction–velocity curves for, clockwise disc speed (◆) and, counter-clockwise disc speed (▲).

$$\mu = \begin{cases} 0{\cdot}42376 - 5{\cdot}76246(V - \dot{y}), & V - \dot{y} \leqslant 0{\cdot}0329 \text{ (m/s)}, \\ -0{\cdot}08144 + 10{\cdot}0133(V - \dot{y}), & V - \dot{y} > 0{\cdot}0329 \text{ (m/s)}, \end{cases} \quad \text{for "CCW"}; \quad (5a)$$

$$\mu = \begin{cases} 2{\cdot}21961 - 94{\cdot}3401(V - \dot{y}), & V - \dot{y} < 0{\cdot}0205 \text{ (m/s)}, \\ 0{\cdot}28195 + 2{\cdot}78858(V - \dot{y}), & V - \dot{y} \geqslant 0{\cdot}0205 \text{ (m/s)}, \end{cases} \quad \text{for "CW"}; \quad (5b)$$

Now the equation of motion according to the cubic non-linear model can be written by substituting relation (4) into equation (1), after multiplying equation (1) by L in the form

$$\ddot{y} + [2\zeta\omega_0 + F_1\alpha(t)]\dot{y} + [\omega_0^2 - \alpha(t)]y + F_2\alpha(t)\dot{y}^2 - F_3\alpha(t)\dot{y}^3 = -F_0\alpha(t), \quad (6a)$$

where $F_0 = L(a_0 - a_1V + a_3V^3)$, $F_1 = L(a_1 - 3a_3V^2)$, $F_2 = 3La_3V$, $F_3 = La_3$.

For convenience of studying the effects of system parameters, the following non-dimensional variables and parameters are introduced:

$$Y = \frac{y}{L}, \quad \tau = \omega_0 t, \quad W(\tau) = \frac{F_0}{L\omega_0^2}\alpha(t).$$

In this case equation (6a) takes the form

$$Y'' + [2\zeta + C_1W(\tau)]Y' + [1 - C_2W(\tau)]Y + C_3W(\tau)Y'^2 - C_4W(\tau)Y'^3 = -W(\tau), \quad (6b)$$

where a prime denotes differentiation with respect to the non-dimensional time parameter τ, and

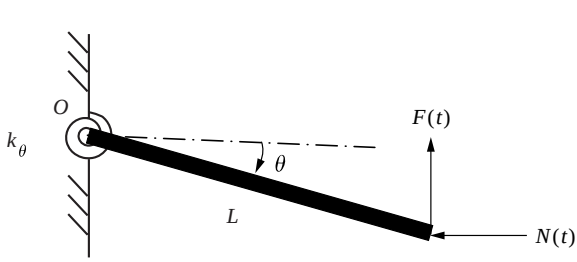

Figure 5. Analytical model of the friction element.

$$C_1 = \frac{F_1}{F_0} L\omega_0, \quad C_2 = \frac{L}{F_0}, \quad C_3 = \frac{F_2}{F_0} L^2\omega_0^2, \quad C_4 = \frac{F_3}{F_0} L^3\omega_0^3.$$

It can be seen that C_1 becomes zero when $V = \sqrt{a_1/3za_3}$ (m/s). For a tangential velocity of the disc lower than $\sqrt{a_1/3a_3}$ (m/s), $C_1 > 0$. If it is greater than $\sqrt{a_1/3a_3}$ (m/s) then $C_1 < 0$. Meanwhile, C_2, C_3 and C_4 are always positive. Note that equation (6b) is a non-linear stochastic differential equation. The non-linearity appears as coefficients to the random parametric excitation of the normal force. This class of systems can be conveniently analyzed using the stochastic averaging method.

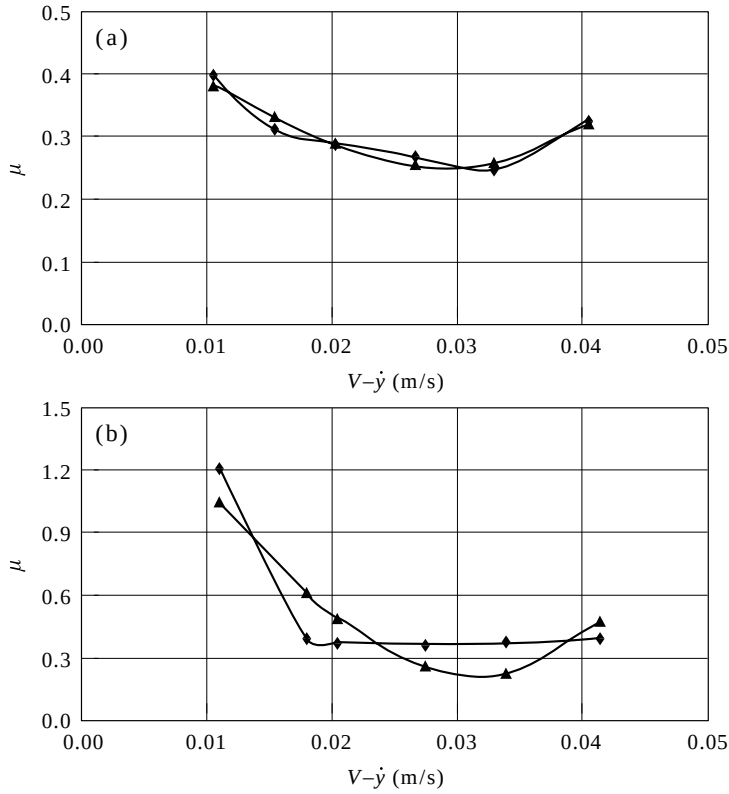

Figure 6. Cubic models of friction coefficient–velocity curves for (a) counter-clockwise disc speed and (b) clockwise disc speed: ◆, test curves; ▲, fitted curves.

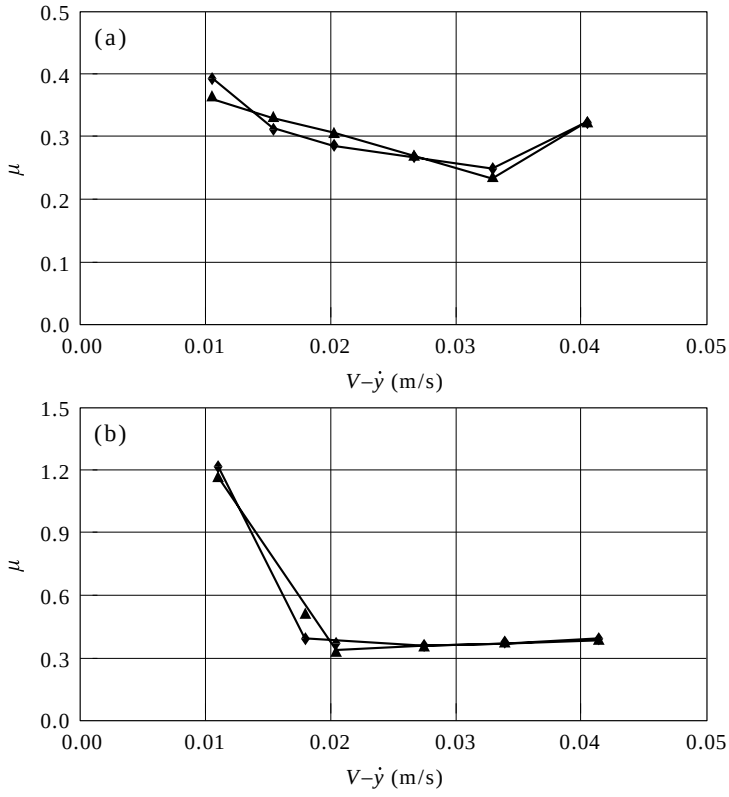

Figure 7. Piecewise linear models of friction coefficient–velocity curves for (a) counter-clockwise disc speed and (b) clockwise disc speed: ◆, test curves; ▲, fitted curves.

4. STOCHASTIC AVERAGING ANALYSIS

4.1. NON-LINEAR FRICTION–VELOCITY MODELLING

The dynamic behavior of the friction element as described by equation (6b) can be analyzed by means of the stochastic averaging method (SAM) established by Stratonovich [14] and mathematically proven by Khasminiskii [15] by his well-known limit theorem. The essence of the method is to replace the response, which contains rapid oscillations due to system non-linearities, by a smooth response described by slowly varying amplitude and phase shift. Usually, the amplitude envelope of the response is uncoupled from the corresponding phase process. When considering only the stationary response, high-frequency oscillations have a localized effect (in time) and do not contribute significantly to the average behavior of the system over a long period of time. The stochastic averaging takes into account the effect of a stochastic parametric process $W(\tau)$ with the multiplied displacement and velocity terms in equation (6b). Equation (6b) involves non-linear terms multiplied by the random process $W(\tau)$. In order to apply the SAM to equation (6b), a standard transformation of variables is introduced in terms of the full amplitude $A(\tau)$ and the full phase angle $\vartheta(\tau)$, as follows:

$$Y(\tau) = A(\tau)\cos\varphi(\tau), \quad Y'(\tau) = -A(\tau)\sin\varphi(\tau), \quad \text{where} \quad \varphi(\tau) = \tau + \vartheta(\tau) \tag{7a}$$

subject to the condition

$$A'\cos\varphi(\tau) - A\vartheta'(\tau)\sin\varphi(\tau) = 0. \tag{7b}$$

Substituting transformation (7a) into equation (6b), using equation (7b), one obtains the following two first-order differential equations:

$$\begin{aligned} A'(\tau) &= -2\zeta A\sin^2\varphi + [1 - C_1 A\sin\varphi - C_2 A\cos\varphi \\ &\quad + C_3 A^2\sin^2\varphi + C_4 A^3\sin^3\varphi]\sin\varphi W(\tau), \\ \theta'(\tau) &= -2\zeta A\sin\varphi\cos\varphi + \left[\frac{1}{A} - C_1\sin\varphi - C_2\cos\varphi \right. \\ &\quad \left. + C_3 A\sin^2\varphi + C_4 A^2\sin^3\varphi\right]\cos\varphi W(\tau), \end{aligned} \tag{8}$$

where $W(\tau)$ is assumed to be stationary bounded random process whose spectrum should be of order ε^2, which is a required condition for the limit theorem. In this case, one can write $W(\tau) = \varepsilon\xi(\tau)$, where $\xi(\tau)$ is also a stationary bounded random process with a mean value m_0 and correlation function $R_\xi(\bar\tau)$, ε is a very small parameter. The damping factor is also very small and can be written according to the small parameter ε as $\zeta = \varepsilon^2\tilde\zeta$. Equations (8) can be written in the standard form

$$A' = \varepsilon^2 f_1(A, \varphi) + \varepsilon g_{11}(A, \varphi)\xi(\tau), \quad \vartheta' = \varepsilon^2 f_2(A, \varphi) + \varepsilon g_{21}(A, \varphi)\xi(\tau), \tag{9a, b}$$

where

$$\begin{aligned} f_1 &= -2\hat\zeta A\sin^2\varphi, \quad f_2 = -2\hat\zeta A\sin\varphi\cos\varphi, \\ g_{11} &= [1 - C_1 A\sin\varphi - C_2 A\cos\varphi + C_3 A^2\sin^2\varphi + C_4 A^3\sin^3\varphi]\sin\varphi, \\ g_{21} &= \left[\frac{1}{A} - C_1\sin\varphi - C_2\cos\varphi + C_3 A\sin^2\varphi + C_4 A^2\sin^3\varphi\right]\cos\varphi. \end{aligned} \tag{10}$$

Both f_i and g_{ij} are periodic functions in τ of period T. If the functions f_i and g_{ij} are sufficiently smooth, the process $\xi(\tau)$ will have a correlation function which decreases as the shift time $\bar\tau \to \infty$. In this case, the solution of equations (9) converges weakly to a diffusive Markov process described by the coupled Itô stochastic differential equations

$$\begin{pmatrix} \mathrm{d}A \\ \mathrm{d}\vartheta \end{pmatrix} = \varepsilon^2 \begin{pmatrix} a_1 \\ a_2 \end{pmatrix} \mathrm{d}\tau + \varepsilon \begin{bmatrix} b_{11} & b_{12} \\ b_{21} & b_{22} \end{bmatrix}^{1/2} \begin{pmatrix} \mathrm{d}B_1(\tau) \\ \mathrm{d}B_2(\tau) \end{pmatrix}, \tag{11}$$

where $B_i(\tau)$ $(i = 1, 2)$ are independent Brownian motion processes with unit variance. The first expression on the right-hand side (with elements a_i) represents the "drift vector" while the square matrix is the "diffusion matrix". The

amplitude $A(\tau)$ and phase $\vartheta(\tau)$ will converge weakly to Markov processes as $\varepsilon \to 0$. The elements of the drift and diffusion expressions of equation (11) are given in Appendix A.

The amplitude equation in equation (11) constitutes a Markov process because it is independent of the phase shift ϑ and its behavior is characterized by a transition probability density $p(A, \tau)$. The time evolution of the response probability density function $p(A, \tau)$ is governed by the well-known Fokker–Planck–Kolmogorov (FPK) equation [16, 17],

$$\frac{\partial p(A,\tau)}{\partial \tau} = -\varepsilon^2 \frac{\partial}{\partial A}\left\{\left[\frac{b_{-1}}{A} + (b_1 - \hat{\zeta})A + b_3 A^3 + b_5 A^5\right] p(A,\tau)\right\} + \frac{\varepsilon^2}{2}\frac{\partial^2}{\partial A^2}\{[b_0 + b_2 A^2 + b_4 A^4 + b_6 A^6] p(A,\tau)\}, \tag{12}$$

where b_i ($i = -1, 0, 1, \ldots, 6$) are constants related to C_i and the spectra $S(j)$ (see Appendix B).

For stationary solution $\partial p(A, \tau)/\partial \tau = 0$, one obtains

$$[a_1(A)p(A,\tau)] - \frac{1}{2}\left[\frac{\partial b_{11}(A)}{\partial A} p(A,\tau) + \frac{\partial p(A,\tau)}{\partial A} b_{11}(A)\right] = 0. \tag{13}$$

The general stationary solution of equation (13) is

$$p(A) = k \frac{e^{\int \frac{2a_1(A)}{b_{11}(A)} dA}}{b_{11}(A)}, \tag{14}$$

where k is the constant of integration which can be determined from satisfying the normalization condition. This condition cannot be found in a closed form due to the degree of non-linearity involved with multiplicative terms. Instead of seeking the probability density of the amplitude A, we will examine the qualitative structure of $p(A)$.

The degree of friction random fluctuations can change the stability properties of the friction element. It is important to establish the stability conditions of the friction element. The interfacial forces can also create new states which never exist under deterministic conditions. One may gain more physical insight to the system dynamic characteristics by studying the friction noise-induced transitions. A transition corresponds to a qualitative change in the state of the system. In order to determine when the system undergoes a transition, one needs to monitor the probability density function (pdf) for qualitative changes. Here, the appropriate indicators of a transition are the extrema of the steady state pdf of the system [16]. The extrema of the response pdf are determined from the system FPK equation by setting $\partial p(A, \tau)/\partial A$ to zero in equation (13). This yields the algebraic equation

$$n_6 A_e^6 + n_4 A_e^4 + n_2 A_e^2 + n_0 = 0, \tag{15}$$

where the roots A_e represent the extrema of the response probability density, and

$$n_0 = b_{-1}, \quad n_2 = b_1 - b_2 - \hat{\zeta}, \quad n_4 = b_3 - 2b_4, \quad n_6 = b_5 - 3b_6,$$

which can be expressed in terms of the system and excitation parameters and are given in Appendix C. Equation (15) has only two real roots given by

$$A_e = \pm \frac{1}{2^{1/6}3^{2/3}} \sqrt{\frac{3^{1/6}n_c}{n_6} - \frac{32^{2/3}\sqrt{3}n_2}{n_c} + \frac{2^{2/3}\sqrt{3}n_4^2}{n_6 n_c} - \frac{6^{1/3}n_4}{n_6}}, \tag{16}$$

where

$$n_c = (9n_6\sqrt{27n_6^2n_0^2 - 18n_6n_2n_0 + 4n_4^3n_0 + 4n_6n_2^3 - n_4^2n_2^2}$$
$$- 27\sqrt{3}n_6^2n_0 + 9\sqrt{3}n_6n_4n_2 - 2\sqrt{3}n_4^3)^{1/3}. \tag{17}$$

In terms of the system and excitation parameters this parameter is given in Appendix D.

Based on the experimental results of the friction spectra, one must select typical values for the spectra at zero frequency, and at non-dimensional frequencies 1 through 4. Since the natural frequency of the system does not remain constant during the test due to time variations of boundary conditions, typical values of the natural frequency were selected ranging from 100 to 150 Hz. The measured spectra were transferred to the non-dimensional one developed in the analytical modelling. Using these typical values of the friction spectra one can analyze the dependence of A_e on friction spectra and different values of disc velocity for clockwise and counter-clockwise cases. The extrema of the clockwise disc rotation are more complicated than those for the counter-clockwise case.

For clockwise disc speed, Figure 8(a) shows the dependence of extrema amplitude A_e on the disc speed for friction element natural frequency $f_0 = 100$ Hz and for three levels of friction spectra $\pi S(0)/\hat{\zeta} = 15$, 17 and 20. The amplitude A_e has non-zero values for disc speed up to 0·0318 (m/s) above which the friction slope becomes positive and the friction element experiences damped oscillations. For $f_0 = 150$ Hz and for each level, Figure 8(b) shows more complicated characteristics, where the extrema are defined by two separate curves for each friction spectral level. The two curves are separated by a region of zero amplitude over a finite region of disc velocity where equation (17) does not possess any real root. The first curve corresponds to low disc velocity up to 0·032 m/s, above which the friction–velocity slope is almost zero, and the system experiences stable equilibrium due to the system damping. This stable equilibrium will be maintained within a small range of disc speed (0·032–0·0358 m/s). There will be a bifurcation at disc speed 0·0358 m/s and the friction element equilibrium position becomes unstable.

For the case of counter-clockwise disc rotation, Figure 9(a) shows the dependence of the amplitude extrema A_e on the disc speed for $f_0 = 100$ Hz and for three levels of friction spectral density $\pi S(0)/\hat{\zeta} = 100$, 130 and 150. The extrema characteristics for this case are different from those studied for the

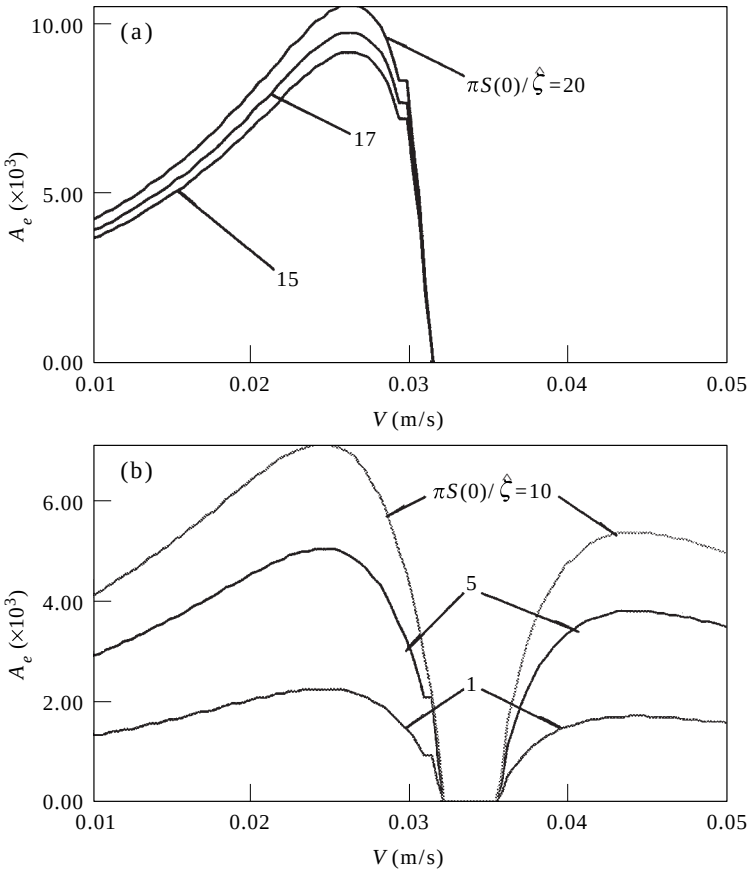

Figure 8. Dependence of the extrema amplitude on the disc speed (clockwise case): (a) friction element natural frequency $f_0 = 100$ Hz, $L\omega_0 = 37{\cdot}7$ m/s, $\zeta = 0{\cdot}01$ and $S(0) = 13S(1) = 85S(2) = 170S(3) = 170S(4)$; (b) friction element natural frequency $f_0 = 150$ Hz, $L\omega_0 = 56{\cdot}6$ m/s, $\zeta = 0{\cdot}01$ and $S(0) = 85S(1) = 165S(2) = 165S(3) = 165S(4)$.

clockwise case. For the present case the disc speed stabilizes the friction element until a critical disc speed where the extrema amplitude reaches its minimum, then the amplitude A_e increases with the disc speed. The destabilizing effect with the disc speed is mainly attributed to the random fluctuations of the contact forces. For $\pi S(0)/\hat{\zeta} = 100$ there exists a small region of disc speed over which the extrema amplitude vanishes. For $f_0 = 150$ Hz the extrema amplitude is continuous with the disc speed. However, it can be seen that the curve corresponding to $\pi S(0)/\hat{\zeta} = 30$ touches the disc speed axis, as shown in Figure 9(b), and if $\pi S(0)/\hat{\zeta} < 30$ then the friction element will experience bifurcation. The bifurcation here signifies a qualitative variation in the system characteristics as the control parameter $\pi S(0)/\hat{\zeta}$ varies. The friction element will experience transition from a stable equilibrium state to fully developed random motion. One should bear in mind that the curves presented in Figures 8 and 9 were obtained for discrete values of friction element natural frequency and friction

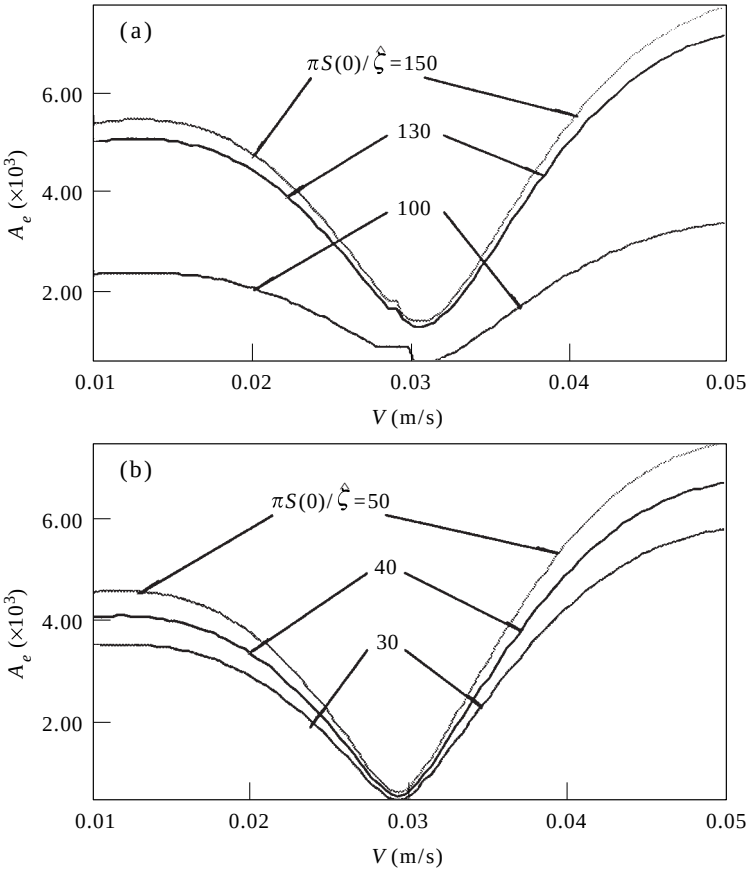

Figure 9. Dependence of the extrema amplitude on the disc speed (counter-clockwise case): (a) friction element natural frequency $f_0 = 100$ Hz, $L\omega_0 = 37{\cdot}7$ m/s, $\zeta = 0{\cdot}01$ and $S(0) = 120S(1) = 650S(2) = 650S(3) = 650S(4)$; (b) friction element natural frequency $f_0 = 150$ Hz, $L\omega_0 = 56{\cdot}6$ m/s, $\zeta = 0{\cdot}01$ and $S(0) = 60S(1) = 60S(2) = 60S(3) = 60S(4)$.

spectral density levels $\pi S(0)/\hat{\zeta}$. On the other hand, the pin boundary conditions at the contact end are time varying. In this case its natural frequency fluctuated during the experimental tests. Note that it was not possible to measure the pin natural frequency during any test. Furthermore, the contact forces are non-stationary random processes in nature, and bifurcation may not be exactly defined by a fixed statistical parameter. One may also conclude that the different forms of brake noise in the form of moan, groan, or squeal may occur simultaneously due to the fact of the non-stationary random fluctuations of contact forces.

4.2. PIECEWISE LINEAR FRICTION–VELOCITY MODELLING

As a special case, by setting $C_3 = C_4 = 0$ in equation (6b), one can obtain modelling for the case of piecewise linear friction–velocity representation described by relations (5). The resulting equation of motion becomes linear non-

homogeneous with one parametric term. This form has been extensively analyzed in the literature [17]. Following the same procedure of SAM, the drift and diffusion coefficients take the form

$$a_1 = \left\{\frac{\pi}{8}[3(C_1^2 + C_2^2)S(2) + 2C_1^2 S(0)] - \hat{\zeta}\right\}A + \frac{\pi}{2A}S(1) = \nu A + \frac{n}{2A}, \tag{18a}$$

$$b_{11} = \left\{\frac{\pi}{4}[(C_1^2 + C_2^2)S(2) + 2C_1^2 S(0)]A^2 + \pi S(1)\right\} = mA^2 + n. \tag{18b}$$

and the stationary pdf can be obtained in the closed form

$$p(A) = \frac{kA}{(mA^2 + n)^{(3/2 - \nu/m)}}, \tag{19a}$$

where k is the constant of integration which is determined from the normalization condition $\int_0^\infty p(A)\,\mathrm{d}A = 1$. This yields the result

$$k = \frac{m - 2\nu}{n^{(\nu/m - 1/2)}} \tag{19b}$$

provided $m > 2v$, which is equivalent to the expression

$$\hat{\zeta} > \frac{\pi}{4}(C_1^2 + C_2^2)S(2), \tag{20}$$

where

$$m - 2\nu = 2\hat{\zeta} - \frac{\pi}{2}(C_1^2 + C_2^2)S(2), \quad n = \pi S(1),$$

$$\nu/m = [(3\pi/8)(C_1^2 + C_2^2)S(2) + (\pi/4)C_1^2 S(0) - \hat{\zeta}] \Big/ [(\pi/4)(C_1^2 + C_2^2)S(2) + (\pi/2)C_1^2 S(0)].$$

Inequality (20) defines the condition of sample stability condition of the amplitude response and also establishes the boundary of bounded solutions as shown in Figures 10(a) and (b) for clockwise and counter-clockwise cases, respectively, and for $f_0 = 100$ Hz. The difference between the two cases is only manifested at lower values of disc speed.

Figures 11(a) and (b) present two sets of the friction element amplitude pdf for the clockwise disc speed case and for two different values of disc speed $V = 0{\cdot}03$ and $0{\cdot}04$ (m/s). Each figure shows the pdf for different values of friction spectral density at twice the system natural frequency $\pi S(2)/\hat{\zeta}$. All the curves follow the typical Raleigh distribution and the peak moves to the right as the friction spectral density level increases. Figures 12(a) and (b) display another two sets of pdf for the counter-clockwise disc speed for the same disc speed values presented in Figures 11(a) and (b). In both cases the friction element amplitude corresponding to the pdf peak moves to the right as the friction spectral density increases.

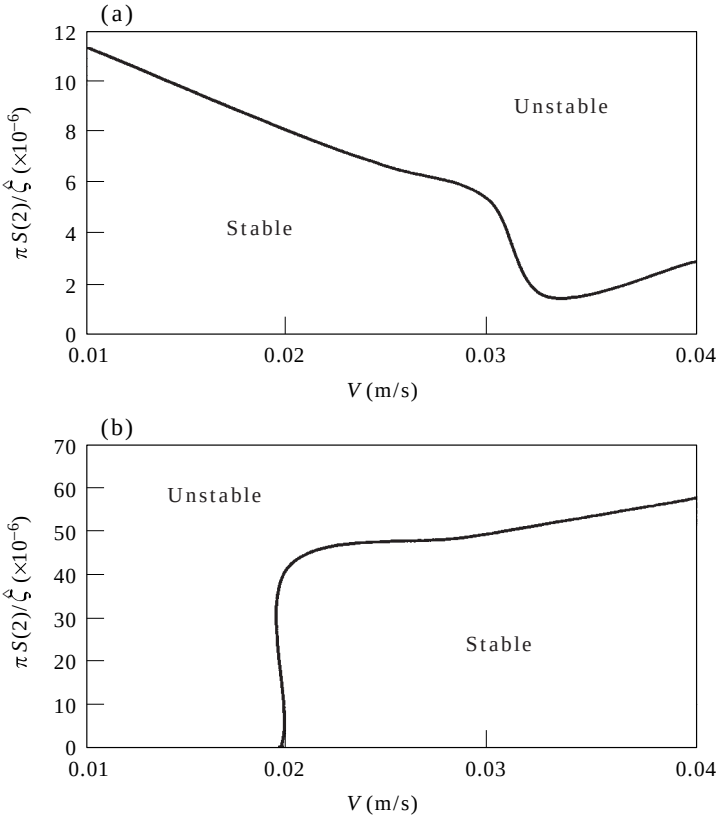

Figure 10. Sample stability boundaries for $f_0 = 100$ Hz: (a) counter-clockwise disc speed; (b) clockwise disc speed.

The nth moment of the amplitude is

$$E[A^i] = \int_0^\infty A^i p(A)\,\mathrm{d}A = \int_0^\infty A^i \left(\frac{m-2\nu}{n^{(\nu/m-1/2)}}\right) \frac{A}{(mA^2+n)^{(3/2-\nu/m)}}\,\mathrm{d}A$$

$$= \frac{B\left(\dfrac{i+2}{2}, -\dfrac{\nu}{m} - \dfrac{i+2}{2} + \dfrac{3}{2}\right) n^{(i+2)/2-1}(m-2\nu)}{2m^{(i+2)/2}}, \tag{21}$$

where $B(p, q) = \int_0^1 x^{p-1}(1-x)^{q-1}\,\mathrm{d}x$ is the Beta function with $\mathrm{Re}(p) > 0$ and $\mathrm{Re}(q) > 0$.

The integral (21) converges if

$$\frac{\nu}{m} < \frac{3}{2} - \frac{i+2}{2}. \tag{21a}$$

Thus, the stability conditions of the first and second moments are, respectively,

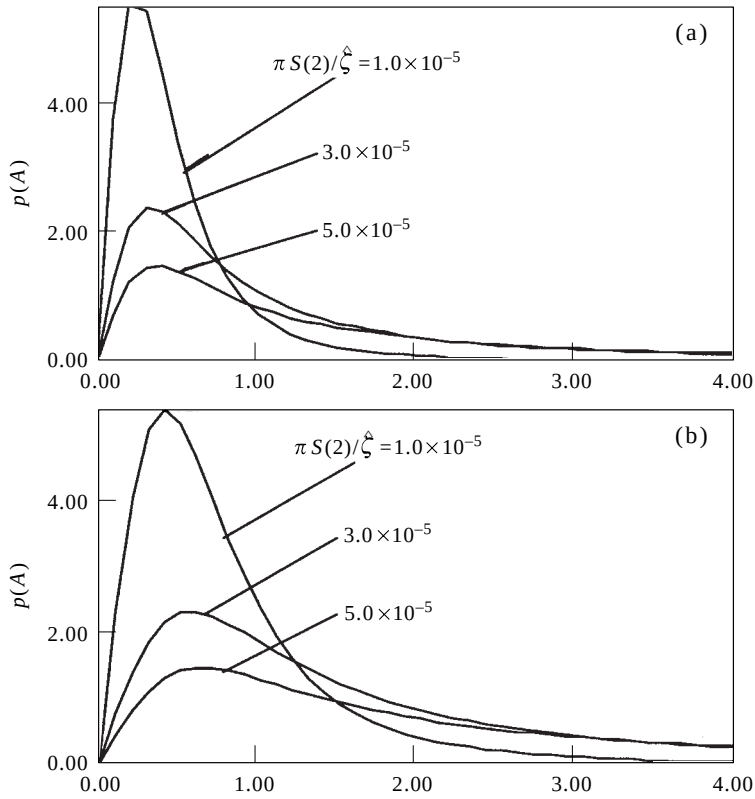

Figure 11. Stationary probability density curves of the friction element amplitude for the case of clockwise disc speed: (a) $V = 0{\cdot}03$ m/s; (b) $V = 0{\cdot}04$ m/s.

$$\nu < 0, \quad \text{i.e.,} \quad \hat{\zeta} > \frac{\pi}{8}[3(C_1^2 + C_2^2)S(2) + 2C_1^2 S(0)], \quad i = 1, \tag{22a}$$

$$2\nu + m < 0, \quad \text{i.e.,} \quad \hat{\zeta} > \frac{\pi}{2}[(C_1^2 + C_2^2)S(2) + C_1^2 S(0)], \quad i = 2. \tag{22b}$$

From equation (21) the mean and mean square of the amplitude are, respectively,

$$E(A) = \frac{B(3/2 - \nu/m)\sqrt{n}(m - 2\nu)}{2m^{3/2}}, \quad E(A^2) = \frac{n(2\nu - m)}{2m^2(1/4 - \nu^2/m^2)} \tag{23}$$

If $C_1 = 0$, which means that the equation of motion (6b) only includes the time variation of the stiffness term and the non-homogeneous term which is due to static friction ($V = \dot{y}$). The stability conditions expressed by equations (20) and (22) are reduced to similar results as those obtained by Roberts [18] for the problem of ship roll motion in random sea waves. These stability conditions establish the levels of contact forces spectra below which the model will not experience any oscillations. Note that the present analysis is based on the

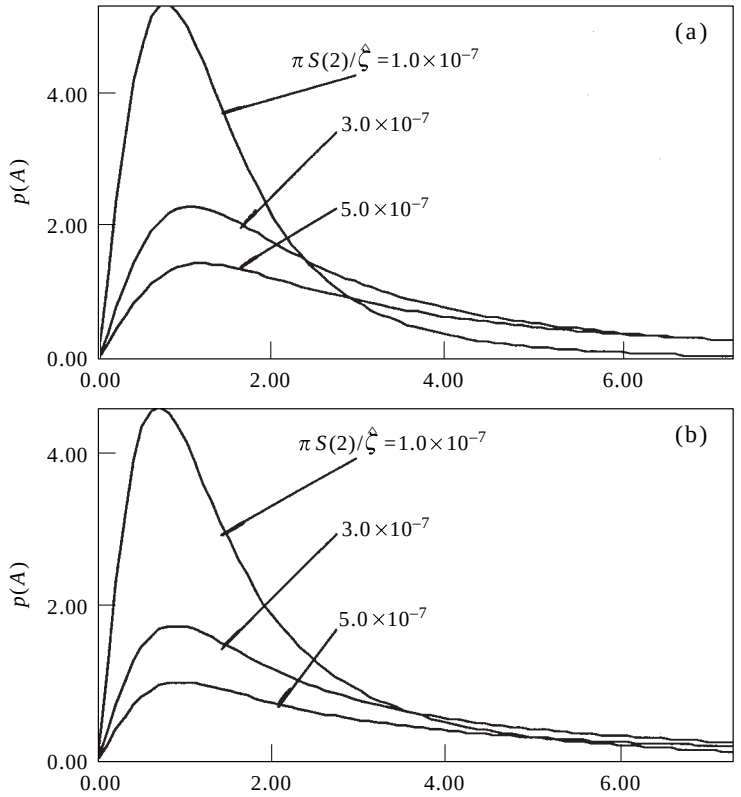

Figure 12. Stationary probability density curves of the friction element amplitude for the case of counter-clockwise disc speed: (a) $V = 0{\cdot}03$ m/s; (b) $V = 0{\cdot}04$ m/s.

assumption that the contact forces are random stationary processes. However, the experimental results showed that these contact forces are non-stationary.

5. CONCLUSIONS

Linear and non-linear phenomenological models have been developed for the interfacial forces between a rotating disc in contact with a rigid pin. In both models the interfacial forces are random, non-stationary, and essentially non-Gaussian. The resulting equation of motion of the non-linear model contains non-linear parametric terms in the velocity terms due to the random fluctuations of the normal force. Due to time variation of boundary conditions, the friction element did not possess constant natural frequency. The analysis of both models was carried out using the stochastic averaging method. The problem of noise-induced transition was analyzed for clockwise and counter-clockwise disc speeds. The amplitude extrema for both cases was plotted in terms of disc velocity and friction spectral density level. The amplitude extrema for the clockwise case was more complicated than the counter-clockwise case due to the sprag-slip phenomenon. For the linear models, closed form solutions of the pin response statistical parameters such as probability density function and

statistical moments were derived in a closed form. The friction statistical parameters for the clockwise case are significantly different from those of the counter-clockwise case. The results of both cases approach each other as the disc speed increases.

ACKNOWLEDGMENT

This research is supported by National Science Foundation Grant No. CMS-9634223, and by the Institute for Manufacturing Research at Wayne State University.

REFERENCES

1. J. P. Den Hartog 1985 *Mechanical Vibrations*. New York: Dover Publications.
2. A. Tondl 1970 *Self-Excited Vibrations*. Monograph No. 9. Bechovice: National Research Institute for Machine Design.
3. C. A. Brockley and P. L. Ko 1970 *ASME Journal of Lubrication Technology* **92**, 550–556. Quasi-harmonic friction-induced vibration.
4. K. Popp and P. Stelter 1990 *Philosophical Transaction of the Royal Society, London* **A 332**, 89–105. Stick-slip and chaos.
5. B. F. Feeny and F. C. Moon 1993 *Journal of Sound and Vibration* **170**, 303–323. Chaos in a forced dry-friction oscillator: experiment and numerical modeling.
6. M. R. North 1976 *Proceedings of the Institution of Mechanical Engineers* **C38/76**, 169–176. Disc brake squeal.
7. R. A. Ibrahim 1994 *ASME Applied Mechanics Reviews* **47**, 227–253. Friction-induced vibration, chatter, squeal, and chaos, part II: dynamics and modelling.
8. J. E. Mottershead, H. Ouyang and M. P. Cartmell 1997 *Proceedings of the Royal Society London A* **453**, 1–19. Parametric resonances in an annular disc, with a rotating system of distributed mass and elasticity; and the effects of friction and damping.
9. A. Filippov 1964 *Differential Equations with Discontinuous Right-Hand Sides*. Rhode. Island: American Mathematical Society Translations **42**, Series 2.
10. P. E. Dupont 1992, *Proceedings of* 1992 *IEEE International Conference on Robotics and Automation*, 1442–1447. The effect of coulomb friction on the existence and uniqueness of the forward dynamics problems.
11. A. H. Dweib and A. F. D'Souza 1990 *Journal of Sound and Vibration* **137**, 163–175, 177–190. Self-excited vibrations induced by dry friction, part I: experimental study–part II: stability and limit cycles.
12. R. T. Spurr 1961 *Proceedings of the Automotive Division, Institute of Mechanical Engineers (AD)* **1**, 33–40. A theory of brake squeal.
13. R. A. Ibrahim, S. Madhavan, S. L. Qiao and W. K. Chang 1998 *International Journal of Vehicle Dynamics* (in press). Experimental investigation of friction-induced noise in disc brake systems.
14. R. L. Stratonovich 1963 *Topics in the Theory of Random Noise*, Vol. I. New York: Gordon & Breach.
15. R. Z. Khasminiskii 1966 *Theory of Probability Applications* **11**, 390–406. A limit theorem for solution of differential equations with random right-hand side.
16. W. Horsthemke and R. Lefever 1989 in *Noise in Nonlinear Dynamical Systems*, Vol. 2 (F. Moss and P. V. E. McClintock, editors) 179–208. Cambridge University Press. Noise-induced transitions (chapter 8).

17. R. A. IBRAHIM 1985 *Parametric Random Vibration*. New York: Wiley.
18. J. B. ROBERTS 1982 *Journal of Ship Research* **26**, 246–253. The effect of parametric excitation on ship rolling in random waves.

APPENDIX A: ESTIMATION OF DRIFT AND DIFFUSION COEFFICIENTS

Consider a set of differential equations of standard form

$$\frac{\mathrm{d}x_i}{\mathrm{d}\tau} = \varepsilon^2 f_1(x, \tau) + \varepsilon \sum_{k=1}^{m} g_{ik}(x, \tau) Z_k(\tau), \quad i = 1, 2, \ldots, n. \tag{A1}$$

If the condition in the standard stochastic averaging method is satisfied, the drift coefficients and diffusion coefficients of the corresponding smooth Itô equations can be evaluated from the expressions

$$a_i(x) = \left\langle f_i(x, \tau) + \sum_{j=1}^{n} \sum_{k=1}^{m} \sum_{l=1}^{m} \int_{-\infty}^{0} \frac{\partial g_{ik}(x, \varphi)}{\partial x_j} g_{ij}(x, \varphi + \bar{\tau}) R_{kl}(\bar{\tau})\, \mathrm{d}\bar{\tau} \right\rangle_{\tau}, \tag{A2}$$

$$b_{ij}(x) = \left\langle \sum_{k=1}^{m} \sum_{l=1}^{m} \int_{-\infty}^{\infty} g_{ik}(x, \varphi) g_{jl}(x, \varphi + \bar{\tau}) R_{kl}(\bar{\tau})\, \mathrm{d}\bar{\tau} \right\rangle_{\tau}. \tag{A3}$$

The notation

$$\langle \cdots \rangle_{\tau} = \lim_{T \to \infty} \frac{1}{T} \int_0^T [\cdots]\, \mathrm{d}\tau$$

denotes a time-averaging operation which may be approximated (over a quasi-period 2π) by

$$\langle \cdots \rangle_{\tau} = \frac{1}{2\pi} \int_0^{2\pi} [\cdots]\, \mathrm{d}\varphi.$$

In the present study, after substituting that $n = 2$ and $m = 1$ in equations (A2) and (A3), the drift coefficients and diffusion coefficients are estimated as follows:

$$a_1 = \frac{1}{T} \int_0^T f_1(A, \varphi)\, \mathrm{d}\varphi + \frac{1}{T} \int_0^T \mathrm{d}\varphi \int_{-\infty}^{0} \left[\frac{\partial g_{11}(A, \varphi)}{\partial A} g_{11}(A, \varphi + \bar{\tau}) + \frac{\partial g_{11}(A, \varphi)}{\partial \varphi} g_{21}(A, \varphi + \bar{\tau}) \right] R(\bar{\tau})\, \mathrm{d}\bar{\tau}$$

$$= -\hat{\zeta}A + \frac{1}{128}\int_{-\infty}^{0}\left\{\frac{64\cos(\bar{\tau})}{A} + [48(C_1^2 + C_2^2)\cos(2\bar{\tau}) + 160C_3\cos(\bar{\tau}) + 32C_1^2]A\right.$$
$$+ [20C_3^2\cos(3\bar{\tau}) + 48C_2C_4\sin(2\bar{\tau}) - 112C_1C_4\cos(2\bar{\tau})$$
$$+ 84C_3^2\cos(\bar{\tau}) - 96C_1C_4]A^3$$
$$\left. + [7\cos(4\bar{\tau}) + 64\cos(2\bar{\tau}) + 54]C_4^2A^5\right\}R_z(\bar{\tau})\,\mathrm{d}\bar{\tau}$$
$$= -\hat{\zeta}A + \frac{\pi}{2A}S(1) + \frac{\pi}{8}[3(C_1^2 + C_2^2)S(2) + 10C_3S(1) + 2C_1^2S(0)]A$$
$$+ \frac{\pi}{32}[5C_3^2S(3) - 28C_1C_4S(2) + 21C_3^2S(1) - 24C_1C_4S(0)]A^3$$
$$+ \frac{C_4^2\pi}{128}[7S(4) + 64S(2) + 54S(0)]A^5, \tag{A4}$$

$$a_2 = \frac{1}{T}\int_0^T f_2(A, \varphi)\,\mathrm{d}\varphi + \frac{1}{T}\int_0^1 \mathrm{d}\varphi\int_{-\infty}^{0}\left[\frac{\partial g_{21}(A, \varphi)}{\partial A}g_{11}(A, \varphi + \bar{\tau})\right.$$
$$\left. + \frac{\partial g_{21}(A, \varphi)}{\partial \varphi}g_{21}(A, \varphi\tau)\right]R(\bar{\tau})\,\mathrm{d}\bar{\tau}$$
$$= \frac{1}{64}\int_{-\infty}^{0}\left\{16[C_1^2 + C_2^2]\sin(2\bar{\tau}) + [8C_3^2\sin(3\bar{\tau}) - 24C_1C_4\sin(2\bar{\tau})\right.$$
$$- 8C_2C_4\cos(2\bar{\tau}) + 8C_3^2\sin(\bar{\tau})]A^2$$
$$\left. + \frac{1}{64}[3\sin(4\bar{\tau}) + 12\sin(2\bar{\tau})]C_4^2A^4\right\}R_z(\bar{\tau})\,\mathrm{d}\bar{\tau}$$
$$= -\frac{\pi}{8}C_2C_4S(2)A^2, \tag{A5}$$

$$b_{11} = \frac{1}{T}\int_0^T \mathrm{d}\varphi\int_{-\infty}^{\infty} g_{11}(A, \varphi)g_{11}(A, \varphi + \bar{\tau})R(\bar{\tau})\,\mathrm{d}\bar{\tau}$$
$$= \frac{1}{128}\int_{-\infty}^{\infty}\{64\cos(\bar{\tau}) + [16(C_1^2 + C_2^2)\cos(2\bar{\tau}) + 96C_3\cos(\bar{\tau}) + 32C_1^2]A^2$$
$$+ [4C_3^2\cos(3\bar{\tau}) - 32C_1C_4\cos(2\bar{\tau}) + 36C_3^2\cos(\bar{\tau}) - 48C_1C_4]A^4$$
$$+ [\cos(4\bar{\tau}) + 16\cos(2\bar{\tau}) + 18]C_4^2A^6\}R_z(\bar{\tau})\bar{\tau}$$

$$= \pi S(1) + \frac{\pi}{4}[(C_1^2 + C_2^2)S(2) + 6C_3S(1) + 2C_1^2S(0)]A^2$$

$$+ \frac{\pi}{16}[C_3^2S(3) - 8C_1C_4S(2) + 9C_3^2S(1) - 12C_1C_4S(0)]A^4$$

$$+ \frac{C_4^2\pi}{64}[S(4) + 16S(2) + 18S(0)]A^6, \tag{A6}$$

$$b_{22} = \frac{1}{T}\int_0^T \mathrm{d}\varphi \int_{-\infty}^{\infty} g_{21}(A, \varphi)g_{21}(A, \varphi + \bar{\tau})R(\bar{\tau})\,\mathrm{d}\bar{\tau}$$

$$= \frac{1}{128}\int_{-\infty}^{\infty} \left\{ \frac{64\cos(\bar{\tau})}{A^2} + [16(C_1^2 + C_2^2)\cos(2\bar{\tau}) + 32C_3\cos(\bar{\tau}) + 32C_2^2] \right.$$

$$+ [4C_3^2\cos(3\bar{\tau}) - 16C_1C_4\cos(2\bar{\tau}) + 4C_3^2\cos(\bar{\tau})]A^2$$

$$\left. + [\cos(4\bar{\tau}) + 4\cos(2\bar{\tau})]C_4^2A^4 \right\} R_z(\bar{\tau})\,\mathrm{d}\bar{\tau}$$

$$= \frac{\pi S(1)}{A^2} + \frac{\pi}{4}[(C_1^2 + C_2^2)S(2) + 2C_3S(1) + 2C_2^2S(0)]$$

$$+ \frac{\pi}{16}[C_3^2S(3) - 4C_1C_4S(2) + C_3^2S(1)]A^2 + \frac{C_4^2\pi}{64}[S(4) + 4S(2)]A^4, \tag{A7}$$

$$b_{12} = b_{21} = 0, \tag{A8}$$

where

$$S(j) = \frac{1}{2\pi}\int_{-\infty}^{\infty} R(\bar{\tau})\cos(j\bar{\tau})\,\mathrm{d}\bar{\tau}, \quad R(\bar{\tau}) = E[\xi(\tau)\xi(\tau + \bar{\tau})], \quad j = 0, 1\ , 3, 4.$$

APPENDIX B: COEFFICIENTS OF EQUATION (12)

$$b_{-1} = \frac{\pi}{2}S(1), \quad b_0 = \pi S(1), \quad b_1 = \frac{\pi}{8}[3(C_1^2 + C_2^2)S(2) + 10C_3S(1) + 2C_1^2S(0)],$$

$$b_2 = \frac{\pi}{4}[(C_1^2 + C_2^2)S(2) + 6C_3S(1) + 2C_1^2S(0)],$$

$$b_3 = \frac{\pi}{32}[5C_3^2S(3) - 28C_1C_4S(2) + 21C_3^2S(1) - 24C_1C_4S(0)],$$

$$b_4 = \frac{\pi}{16}[C_3^2S(3) - 8C_1C_4S(2) + 9C_3^2S(1) - 12C_1C_4S(0)],$$

$$b_5 = \frac{C_4^2\pi}{128}[7S(4) + 64S(2) + 54S(0)], \quad b_6 = \frac{C_4^2\pi}{64}[S(4) + 16S(2) + 18S(0)].$$

APPENDIX C: COEFFICIENTS OF EQUATION (15)

$$n_6 = \frac{C_4^2\pi}{128}[S(4) - 32S(2) - 54S(0)],$$

$$n_4 = \frac{\pi}{32}[C_3^2 S(3) + 4C_1C_4S(2) - 15C_3^2S(1) + 24C_1C_4S(0)],$$

$$n_2 = \frac{\pi}{8}[(C_1^2 + C_2^2)S(2) - 2C_3S(1) - 2C_1^2S(0)] - \hat{\zeta}, \quad n_0 = \frac{\pi}{2}S(1).$$

APPENDIX D: RELATION (17) IN TERMS OF SYSTEM AND EXCITATION PARAMETERS

$$\begin{aligned}
n_c = \Bigg\{ & 9\pi C_4^2[S(4) - 32S(2) - 54S(0)]\Bigg[\frac{27\pi^4C_4^4S(1)^2[S(4) - 32S(2) - 54S(0)]^2}{65\,536} \\
& - 9\pi^3C_4^2S(1)\frac{1}{4096}[C_3^2[S(3) - 15S(1)] + 4C_1C_4[S(2) + 6S(0)]\Bigg] \\
& \times \left[\frac{\pi}{8}(C_1^2 + C_2^2)S(2) - \frac{\pi}{4}C_3S(1) - \frac{\pi}{4}C_1^2S(0) - \hat{\zeta}\right][S(4) - 32S(2) - 54S(0)] \\
& + \frac{\pi^4}{16\,384}S(1)[C_3^2[S(3) - 15S(1)] + 4C_1C_4[S(2) + 6S(0)]]^3 \\
& + \pi C_4^2\frac{1}{32}[S(4) - 32S(2) - 54S(0)] \\
& \times \left[\frac{\pi}{8}(C_1^2 + C_2^2)S(2) - \frac{\pi}{2}C_3S(1) - \frac{\pi}{4}C_1^2S(0) - \hat{\zeta}\right]^3 \\
& - \pi^2\frac{1}{1024}[C_3^2[S(3) - 15S(1)] + 4C_1C_4[S(2) + 6S(0)]]^2 \\
& \times \left[\frac{\pi}{8}(C_1^2 + C_2^2)S(2) - \frac{\pi}{4}C_3S(1) - \frac{\pi}{4}C_1^2S(0) - \hat{\zeta}\right]^2\Bigg]^{1/2} \\
& - \frac{27\sqrt{3}\pi^3C_4^4S(1)[S(4) - 32S(2) - 54S(0)]^2}{32\,768} \\
& + 9\sqrt{3}\pi^2C_4^2[S(4) - 32S(2) - 54S(0)] \\
& [C_3^2[S(3) - 15S(1)] + 4C_1C_4[S(2) + 6S(0)]] \\
& \times \frac{\left[\frac{\pi}{8}(C_1^2 + C_2^2)S(2) - \frac{\pi}{4}C_3S(1) - \frac{\pi}{4}C_1^2S(0) - \hat{\zeta}\right]}{4096} \\
& - \frac{\sqrt{3}\pi^3[C_3^2[S(3) - 15S(1)] + 4C_1C_4[S(2) + 6S(0)]]^3}{16\,384}\Bigg\}^{1/3}.
\end{aligned}$$